

Electronic Supplementary Information

Effect of Trap States on Photocatalytic Properties of Boron-doped Anatase TiO₂ Microspheres Studied by Time-resolved Infrared Spectroscopy

Yijie Du,^{ab} Zhuan Wang,^{*a} Hailong Chen,^a Hao-Yi Wang,^a Gang Liu,^{cd} and Yuxiang Weng^{*ab}

^a The Key Laboratory of Soft Matter Physics, Beijing National Laboratory for Condensed Matter Physics, Institute of Physics, Chinese Academy of Sciences, Beijing 100190, China

^b School of Physical Sciences, University of Chinese Academy of Sciences, Beijing 100049, China

^c Shenyang National Laboratory for Materials Science Institute of Metal Research, Chinese Academy of Sciences, 72 Wenhua Road, Shenyang 110016, China

^d School of Materials Science and Engineering, University of Science and Technology of China, 72 Wenhua Road, Shenyang 110016, China

* To whom all correspondence should be addressed: zhuanwang@iphy.ac.cn, and yxweng@aphy.iphy.ac.cn.

Content:

Supplementary Text

1. Transient Infrared Absorption-Excitation Energy Scanning Spectroscopy
2. Femtosecond Time-Resolved IR Spectroscopic Measurements
3. Descriptions of the multi-exponential decay fitting
4. Modelling description for the global fitting

Supplementary Fig. S1 to S9

Supplementary Table S1 to S2

References

Supplementary Text

1. Transient Infrared Absorption-Excitation Energy Scanning Spectroscopy

The TIRA-EESS apparatus were used to characterize the spectra of photocatalysts and monitor the kinetics behavior of photogenerated electrons. As shown in Fig. S1, the excitation laser pulses were from an optical parametric oscillator (OPO, GWU premiScan-ULD/240, Spectra Physics) and optical frequency mixer (uvScan, Spectra Physics) which is pumped by the 355 nm laser pulses delivered from a Nd:YAG laser (Quanta Ray, Spectra Physics) with a pulse duration of 10 ns and a repetition rate of 10 Hz.^{1,2} A quantum cascade laser (Daylight Solutions) was employed as a probe light, which is a continuous wave semiconductor laser with an output wavelength tunable from 4.69 to 4.88 μm (2050 to 2130 cm^{-1}). In this experiment, the wavelength of the probe was set to be 2090 cm^{-1} . A metal wire grid was used to adjust the intensity of mid-infrared probe light. The transmitted mid-infrared beam was detected by a Mercury-Cadmium-Telluride (MCT) detector (Kolmar Technologies, KV104-0.5-A-2/8). Then the photocurrent was amplified by a current preamplifier (Kolmar Technologies, KA020-A1) and filtered by a low band pass filter (Beijing Daze, 20 MHz-DC). Next, the output signal was acquired by a digital oscilloscope (Tektronix, MSO3054C). Finally, the acquired data was transferred to the personal computer.

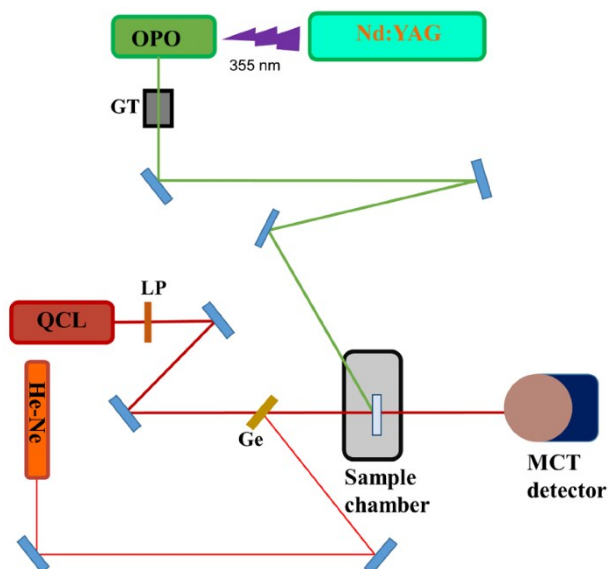


Fig. S1 Microsecond time-resolved transient infrared absorption-excitation energy scanning spectrometers. A: attenuator; F: filter; GT: Glan-Taylor polarizer; P: pinhole; M: mirror; L: len; LP: long pass filter; Ge: germanium window; WG: wire grid; QCL: quantum cascade laser.

2. Femtosecond Time-Resolved Spectroscopic Measurements

As shown in Fig. S2, the laser source is a Ti:Sapphire femtosecond amplifier laser (Spitfire Ace, Spectra Physics) which delivers 800 nm centered laser pulses with a duration of 35 fs (FWHM) at a repetition rate of 1 kHz. The 800 nm laser pulses were split into two beams. One beam was reflected by the beam splitter and guided to the optical parameters amplifier (TOPAS, Spectra Physics) to generate the pump light. The other beam is used to generate the super-continuum (covering the visible and mid-IR spectral range) probe light.³ Specifically, a BBO crystal was used to generate 400 nm pulse and then the fundamental and second harmonic pulses were separated with a harmonic separator. These two beams were combined and focused into air. By finely tuning the delay between these two beams to zero with a manual stage, the mid-IR continuum was generated. A computer-controlled delay line was introduced in the pump beam to change the delay between the pump and the probe pulses.

During the femtosecond time-resolved mid-IR spectroscopy experiment, the pump pulses were modulated by a mechanical chopper at a frequency synchronized to the half of the laser repetition rate. A germanium wafer was used to filter out the visible light. The transmitted transient mid-IR signals were collected by a spectrometer (iHR 320, HORIBA Jobin Yvon) and acquired by a liquid-nitrogen-cooled 64-channel mercury-cadmium-telluride (MCT) array detector (FPAS-0144, Infrared Systems Development). The central wavelength of the spectrometer grating was set to be 5000 nm since the signal to noise ratio was the best for the system.

The time-resolved transient absorption in the visible region was conducted in the

diffuse reflection mode. A variable metallic neutral density filter was employed to filter out the mid-IR and tune the intensity of the probe to the visible light. The diffused probe light was collected by a home-built 46-channel lock-in amplifier assisted spectrometer and then detected by a 46-pixel Si photodiode array. Finally, the acquired data was transferred to the personal computer. Owing to strong scattering of the probing white light, the transient reflection in the visible range (580 nm -720 nm) was acquired with a signal to noise ratio better than 5×10^{-4} . The kinetics at 630 nm was plotted in Fig. S4.

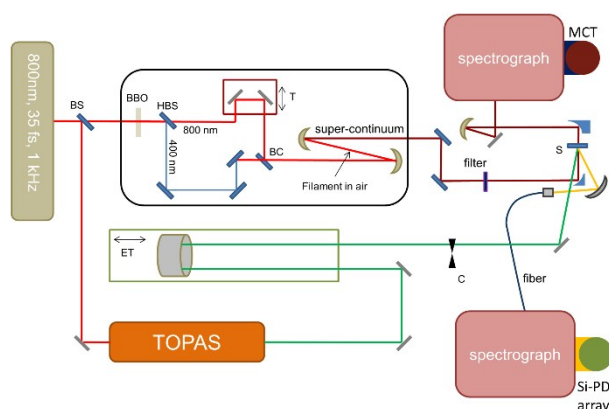


Fig. S2 Femtosecond time-resolved transient infrared absorption spectrometers. BS: beam splitter; HBS: harmonic beam splitter; BC: dichroscope; S: sample chamber; T: translation manual stage; ET: electric translation stage; C: chopper; Si-PD: silicon photodiode.

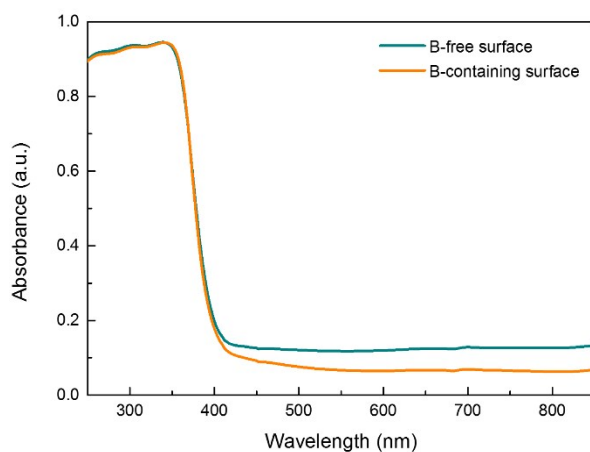


Fig. S3 UV-visible absorption spectra of B-free surface and B-containing surface TiO₂ microspheres.

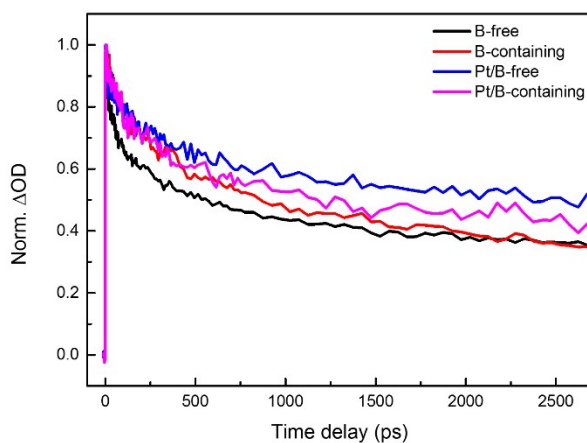


Fig. S4 Normalized decay curves assigned to the absorption of photogenerated holes for B-free surface and B-containing surface TiO₂ with and without co-catalyst platinum loaded on the surface. The decay curves were excited by 360 nm laser and measured at 630 nm. Excitation condition: 200 nJ/pulse.

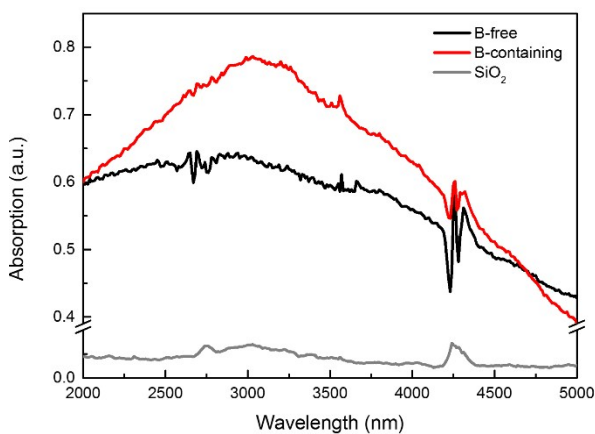


Fig. S5 Steady state IR absorption spectra of B-free (black), B-containing (red), surface TiO₂. The absorption spectra of SiO₂ microsphere powder (gray) was also listed for comparison.

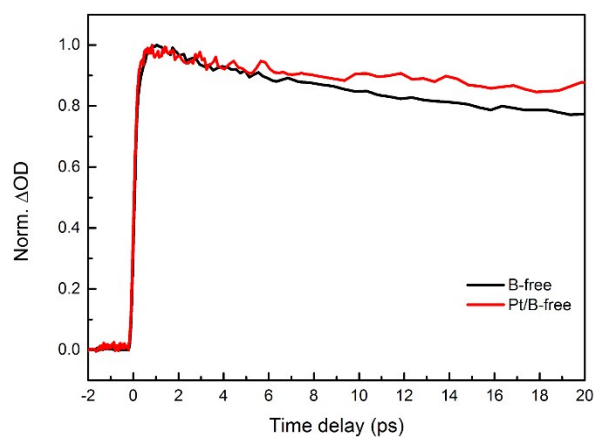


Fig. S6 Normalized TAS decay curves of B-free surface TiO₂ with and without co-catalyst platinum loaded on the surface. The decay curves were excited by 360 nm laser and measured at 5000 nm. Excitation condition: 200 nJ/pulse.

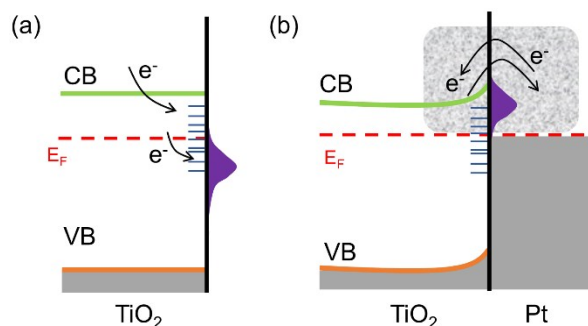


Fig. S7 Schematic illustration for relaxation effect of photogenerated electrons (a) without and (b) with Pt loaded on the TiO₂ surface.

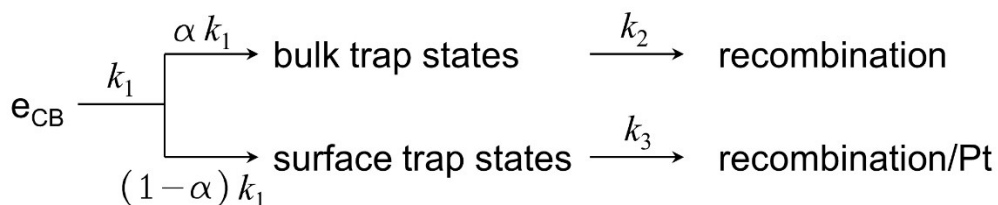
3. Descriptions of the multi-exponential decay fitting

In this work, all measured temporal evolution of the excitation-induced absorption change $\Delta OD(t)$ can be well fitted by a double exponential decay function convoluted with an instrument response function (IRF), i.e., $\Delta OD(t) = [A_1 \cdot \exp(-t/\tau_1) + A_2 \cdot \exp(-t/\tau_2)] \oplus i(t)$, where \oplus represents the convolution, τ_1 , τ_2 are time constants, A_1 , A_2 are corresponding pre-exponential factors, and $i(t)$ is a Gaussian function of IRF with the full width at half maximum about 150 fs.

4. Modelling description for the global fitting

Fig. S8-9 show both the models and the global fitting results of the (Pt loaded) boron-doped TiO₂ (Fig. S8: B-free; Fig. S9: B-containing). After the global fitting, *species associated difference spectra* and their corresponding *population evolution kinetics* are presented. In these models for (Pt loaded) boron-doped TiO₂, we assume that the photogenerated electrons are first excited to the CB after the light absorption, then the majority of the photogenerated electrons will relax to the bulk trap states and undergo charge recombination while the remaining part of the electrons will migrate to the surface trap states and undergo either charge recombination or transfer to the Pt (we

do not consider the possible very fast electron transfer process from TiO₂ to Pt, i.e., ca. 0.2 ps due to the limit of the temporal resolution of the light scattering samples). The procedures can be described by the following scheme^{4,5}:



where α is the proportion coefficient of the photogenerated electrons relaxing to the bulk trap states. According to the literature⁶, the majority of the electrons will recombine in the bulk after the photoexcitation. Therefore, we assume the value α of to be 70% in our model. The fitting rate constants are summarized in **Table S2**.

Based on **Table S2**, we first compared $1/k_1$, $1/k_2$ for both the B-free and B-containing samples, which shows that both $1/k_1$, $1/k_2$ are obviously larger in the latter, suggesting that both the charge trapping and recombination processes are faster at either the surface or the bulk, consistent to the fact that boron doping at the shell creates more charge recombination centers. Then we compared $1/k_3$ for the Pt loaded samples with their counterpart unloaded ones. We found that $1/k_3$ is smaller by a factor of 2 when B-free sample is loaded with Pt, suggesting that owing to the equilibrium built between Pt and TiO₂, the charge recombination has been significantly retarded. On the other hand, the difference of $1/k_3$ between B-containing samples with load and unload of Pt, their ratio is less than 1.2, suggesting that Pt almost has no effect on the surface charge recombination rate, i.e., surface boron prevent an efficient electron transfer from TiO₂ to Pt. Finally, we compared the species associated spectra of Pt-loaded samples with

those of unloaded samples, the results show that the all the spectra of the photogenerated electrons in CB and those trapped at the surface are red-shifted after loaded with Pt. This is consistent with the band-bending effect of Pt described in **Fig. S7**, which has been explained in the context.

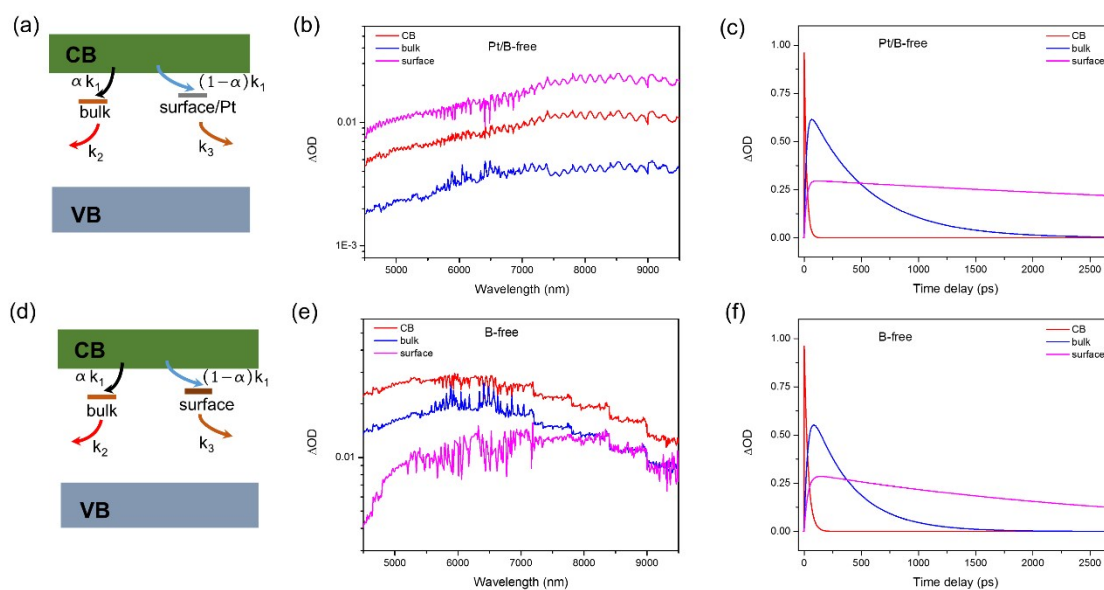


Fig. S8 Global fitting results of the Pt loaded B-free (Pt/B-free) surface TiO₂ (a-c) and B-free surface TiO₂ (d-f). (a) Schematic model for different charge recombination pathways of Pt/B-free surface TiO₂. Black and blue arrows represent CB electrons relaxing to the TiO₂ bulk and surface trap states, respectively. Red arrow represents the charge recombination process in the bulk states and the brown arrow represents the charge recombination in the surface states and/or transfer to Pt subsequently. (b) The corresponding transient species associated spectra and (c) their corresponding kinetics in Pt/B-free surface TiO₂. CB (red line): photogenerated electrons; bulk (blue line): trapped electrons in the bulk states; surface (magenta line): trapped electrons in the surface states. (d) Schematic model for different charge recombination pathways of B-free surface TiO₂. (e) The corresponding transient species associated spectra and (f) their corresponding kinetics in B-free surface TiO₂.

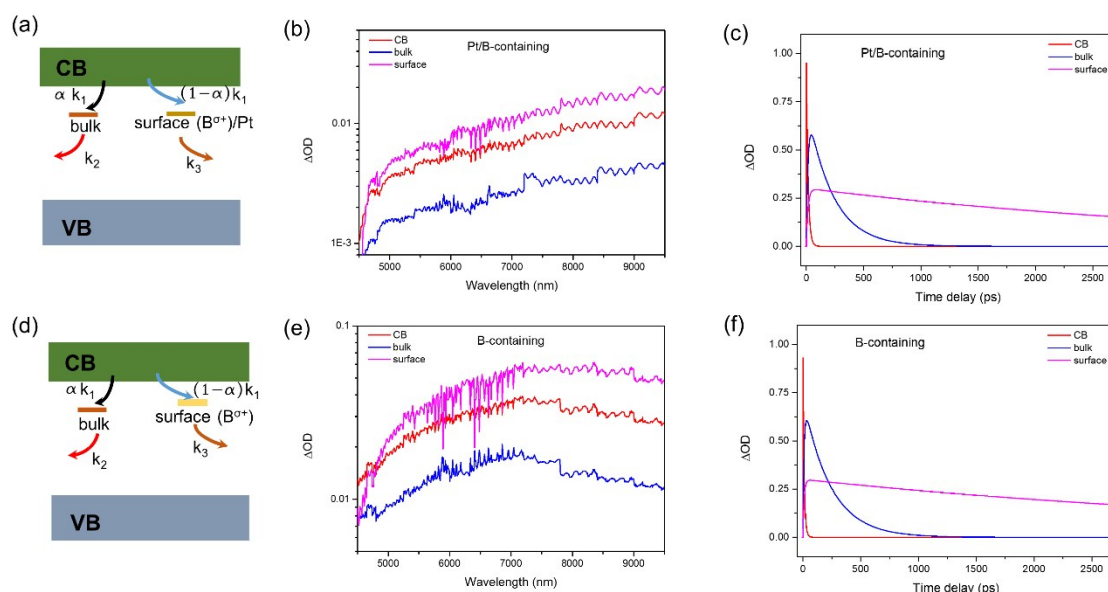


Fig. S9 Global fitting results of the Pt loaded B-containing (Pt/B-containing) surface TiO₂ (a-c) and B-containing surface TiO₂ (d-f). (a) Schematic model for different charge recombination pathways of Pt/B-containing surface TiO₂. Black and blue arrows represent CB electrons relaxing to the TiO₂ bulk and surface trap states, respectively. Red arrow represents the charge recombination process in the bulk states and the brown arrow represents the charge recombination in the surface states and/or transfer to Pt subsequently. (b) The corresponding transient species associated spectra and (c) their corresponding kinetics in Pt/B-containing surface TiO₂. CB (red line): photogenerated electrons; bulk (blue line): trapped electrons in the bulk states; surface (magenta line): trapped electrons in the surface states. (d) Schematic model for different charge recombination pathways of B-containing surface TiO₂. (e) The corresponding transient species associated spectra and (f) their corresponding kinetics in B-containing surface TiO₂.

Table S1 Fitting time constants for nanosecond time-resolved results under different excitation wavelength.

| Samples | wavelength (nm) | τ_1 (μ s) | τ_2 (μ s) |
|--------------|-----------------|---------------------|---------------------|
| B-free | 370 | 0.33 ± 0.01 | 6.8 ± 0.1 |
| B-containing | | 0.26 ± 0.01 | 55.4 ± 2.8 |
| B-free | 410 | 0.61 ± 0.01 | 13.8 ± 0.6 |
| B-containing | | 0.46 ± 0.08 | 53.9 ± 13.1 |
| B-free | 600 | 0.66 ± 0.05 | 13.9 ± 1.2 |
| B-containing | | - | - |

Table S2 Time constants fitted from the global fitting for the different TiO₂ samples.

| Samples | $1/k_1$ (ps) | $1/k_2$ (ps) | $1/k_3$ (ps) |
|-----------------|--------------|--------------|--------------|
| B-free | 33 | 378 | 4131 |
| Pt/B-free | 19 | 516 | 8430 |
| B-containing | 10 | 253 | 4000 |
| Pt/B-containing | 14 | 222 | 4666 |

References

- S1. Y. Mi and Y. Weng, *Sci. Rep.*, 2015, **5**, 11482.
S2. M. Zhu, Y. Mi, G. Zhu, D. Li, Y. Wang and Y. Weng, *J. Phys. Chem. C*, 2013, **117**, 18863-18869.
S3. Y. Nomura, H. Shirai, K. Ishii, N. Tsurumachi, A. A. Voronin, A. M. Zheltikov and T. Fuji, *Opt. Express*, 2012, **20**, 24741-24747.
S4. A. L. Linsebigler, G. Q. Lu and J. T. Yates, *Chem. Rev.*, 1995, **95**, 735-758.
S5. T. Hisatomi, J. Kubota and K. Domen, *Chem. Soc. Rev.*, 2014, **43**, 7520-7535.
S6. M. Sachs, E. Pastor, A. Kafizas and J. R. Durrant, *J. Phys. Chem. Lett.*, 2016, **7**, 3742-3746.